

## The microstructure and mechanical performance of high strength alloy steel X2M

K. Manigandan<sup>1</sup>, T.S. Srivatsan<sup>\*1</sup>, A.M. Freborg<sup>2</sup>,  
T. Quick<sup>3</sup> and S. Sastry<sup>1</sup>

<sup>1</sup>Department of Mechanical Engineering, The University of Akron Akron, Ohio 44325

<sup>2</sup>Department of Geology, The University of Akron Akron, Ohio 44325

<sup>3</sup>Deformation Control Technology, Inc. 7261 Engle Rd., Suite 105 Cleveland, OH 44130

(Received November 5, 2013, Revised March 23, 2014, Accepted April 4, 2014)

**Abstract.** In this paper, the microstructure, hardness, tensile deformation and fracture behavior of high strength alloy steel X2M is presented and discussed. The influence of both composition and processing on microstructure of the as-provided material and resultant influence of microstructure, as a function of orientation, on hardness, tensile properties and final fracture behavior is highlighted. The macroscopic mode and intrinsic microscopic features that result from fracture of the steel specimens machined from the two orientations, longitudinal and transverse is discussed. The intrinsic microscopic mechanisms governing quasi-static deformation and final fracture behavior of this high strength steel are outlined in light of the effects of test specimen orientation, intrinsic microstructural effects and nature of loading.

**Keywords:** composition; processing (carburization); orientation; microstructure; hardness; tensile properties and fracture behavior

---

### 1. Introduction

In more recent years, important advances in the specific domain of alloy engineering have been successfully used to enhance both strength and fatigue characteristics in advanced aerospace and other related technological innovations and concomitant applications. Concurrently, an increased emphasis and importance related to the industries of aerospace, power generation and even automotive, is pushing this technology to new limits that is largely dictated by both commercial and military interests. This has certainly provided the desired interest and impetus for developing new, improved and advanced metal alloys as viable replacements and/or alternatives to the materials currently being used. This particular aspect has been shown and neatly described in the published literature by several researchers in recent years (Thomas *et al.* 1965, Pascover and Makas 1965, Van Slycken *et al.* 2006, Van Slycken *et al.* 2007, Danzeisen *et al.* 2008). Both prevailing and emerging technology requirements continue to place an increased emphasis on issues like off-the shelf availability, lower weight, damage tolerance, durability, fabricability, high life-cycle

---

\*Corresponding Author, Ph.D Student., E-mail: [srivatsants@yahoo.com](mailto:srivatsants@yahoo.com)

performance and even cost effectiveness as primary considerations in governing not only the development of materials but also in their selection and use for a given application. Also, Bucker *et al.* 1966 and Averbach *et al.* 1985 have recorded this observation in the published literature based on findings of their exhaustive independent study.

The need to focus on materials that could offer an attractive combination of high specific strength ( $\sigma/\rho$ ) and superior corrosion resistance coupled with noticeable innovations in processing techniques, spanning the domains of both primary and secondary, have made possible the ease of manufacturing specialty steel, which provides a combination of good strength, acceptable ductility and fracture toughness. A similar view point was also put forth in the published literature by Bajer *et al.* 1965, Cunningham 1975 and Averbach, *et al.* 1985.

A minor modification to the hot worked die steel H-12 (AISI) by way of reduction in carbon content to 0.15 pct. coupled with carburization resulted in a steel that was named X2M. This was initially determined and put forth in print by Averbach *et al.* 1985. The carburized X2M steel was initially used for high performance gears that were put to use for helicopters of the US Army. This observation was also found and recorded in the published literature by two other independent researchers (Cunningham 1974 and Townsend *et al.* 1980). Besides, this steel was also being used for other critical U.S. Army rotor craft power train components. Selection and use in such components necessitated the need to evaluate the synergistic influence of composition, processing and microstructure on fatigue resistance and fracture toughness of the material. Metal manufacturers found this steel difficult to carburize than competing steels on account of the tendency to form massive carbides at the surface. This aspect was initially shown and recorded in the published literature during the mid-1970s (Cunningham 1975). Sustained research and development efforts did eventually lead to successful carburization coupled with a good concentration of carbon (Cunningham 1974).

The purpose of this paper is to present and discuss the intrinsic influence of alloy chemistry and carburization on microstructure development, indentation resistance or hardness and tensile response, by way of properties and final fracture behavior, of this alloy steel. A rationalization of the tensile fracture behavior of this alloy steel is made in light of the synergistic and mutually interactive influences of intrinsic microstructural effects and nature of loading.

## 2. Material

The alloy steel, denoted as X2M, has a chemical composition given in Table 1. The steel was produced using a combination of vacuum induction melting and vacuum arc re-melting (VIM-VAR) by Teledyne Vasco. The presence of carbon provides solid solution strengthening while concurrently enabling a noticeable enhancement in hardenability through the formation and presence of alloy carbides in the microstructure. The alloy carbides provide enhanced strength to the steel. The presence of chromium (Cr), molybdenum (Mo), tungsten (W) and Vanadium (V) results in the formation and presence of alloy carbides, which either directly or indirectly contribute to increasing the strength of the steel matrix. Typically, this alloy steel is carburized in an atmosphere of nitrogen-methanol natural gas at 955°C [1750 F] and controlled by means of a probe. In striving to keep pace with the demands posed by technological innovations, vacuum carburizing has emerged as a viable and attractive alternative to traditional carburizing. The alloy steel that has been characterized in this study was the non-carburized base metal, representing the tough, fatigue resistant core having a predominantly alloy carbide structure.

Table 1 Nominal chemical composition of alloy steel X-2M (in weight percent)

Element	C	Mn	Si	Cr	Mo	V
Percentage	0.14	0.5	0.9	5	1.4	0.5

### 3. Experimental procedures

#### 3.1 Microstructural characterization

Samples of the steel taken from both the longitudinal (L) and transverse (T) orientations were prepared very much in conformance with standard procedures used for the metallographic preparation of metal samples. This involved coarse polish using progressively finer grades of silicon carbide (SiC) impregnated emery paper [i.e., 320-, 400- and 600-grit] followed by fine polishing using 5 micron and 1 micron alumina-based polishing compound suspended in distilled water as the lubricant. The as-polished samples were then etched using nital reagent, i.e., a solution mixture of nitric acid in methanol. Etching helps in revealing the grain boundaries, morphology of the grains, and other intrinsic features in the microstructure. The polished and etched samples were examined in an optical microscope, at low magnifications, and photographed using standard bright field illumination technique.

#### 3.2 Hardness testing

A basic mechanical property of a material is its hardness. The hardness test is an important and widely used test for the purpose of quickly evaluating the mechanical properties of monolithic metals, their alloy counterparts, and even composite materials based on metal matrices. A simple yet appropriate definition that has been recorded for hardness is the resistance offered by the material to indentation, i.e., permanent deformation and cracking (Askeland and Phulke 2005). A direct measurement of hardness is both a simple and useful technique for characterizing the base-line mechanical properties while concurrently investigating, establishing and rationalizing the role and contribution of intrinsic microstructural constituents. Overall, the hardness test can be safely considered to be both simple and easy enough to enable it to be safely categorized as being non-destructive (Askeland and Phulke 2008 and Dieter 1986). In this study, the Vickers micro-hardness ( $H_V$ ) measurements were made on a microhardness tester using an indentation load of 500 grams, a dwell time of 15 seconds, with the aid of a Vickers tool indenter. The indenter (made of diamond) has a square-base pyramidal geometry with an included angle of 136 degrees. The indenter rests for a specified length of time on the polished surface of the test specimen. The machine makes an indent, or impression, on the polished surface of the sample whose diagonal size was measured using a low magnification optical microscope. The area of the impression is directly proportional to the load used and a load independent hardness number can be found. The Vickers hardness number ( $H_V$ ) is the ratio of applied load to the surface area of the indent and was provided by the test machine. Three indents were made edge-to-edge across the polished surface of both the longitudinal and transverse samples of alloy steel X2M, and the result is reported as the average value in units of  $\text{kg/mm}^2$ .

### **3.3 Mechanical testing**

Cylindrical test specimens, conforming to specifications outlined in ASTM E-8-06 (American Society for Testing Material 2006), were precision machined from the chosen steel. The threaded test specimens measured 59 mm in length and 6.35 mm in diameter at the thread section. The gage section of the machined test specimen measured 12.5 mm in length and 3.175 mm in diameter. To minimize the effects of surface irregularities and finish, the gage sections of the machined test specimens were mechanically ground using progressively finer grades of SiC impregnated emery paper. The purpose of polishing was to remove any and all circumferential scratches and surface machining marks.

Uniaxial tensile tests were performed up until failure on a fully-automated, closed-loop servohydraulic mechanical test machine [INSTRON Model 8500 plus] equipped with a 100KN load cell. The test specimens were deformed at a constant strain rate of 0.0001/sec. An axial 12.5 mm gage length extensometer was attached to the test specimen at the gage section, using rubber bands, to provide a precise measurement of strain during uniaxial loading and resultant stretching of the test specimen. The stress and strain measurements, parallel to the load line, were recorded on a PC-based data acquisition system [DAS].

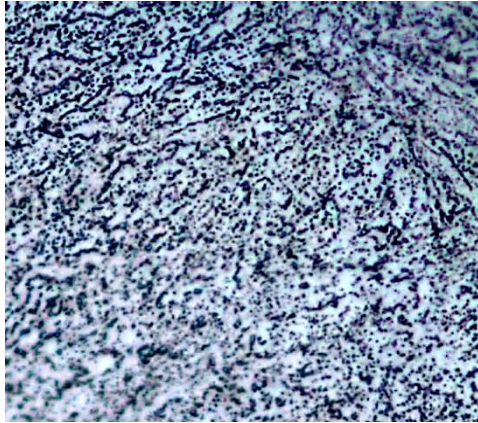
### **3.4 Failure-damage analysis**

Fracture surfaces of the steel samples that were deformed and failed in tension were carefully examined in a scanning electron microscope (SEM) to determine the macroscopic fracture mode and to concurrently characterize the fine scale topography of the tensile fracture surface that would help establish the microscopic mechanisms governing tensile fracture. This is especially important given the alloy carbides unique to this high performance steel. The macroscopic mode refers to the overall mode of failure, while microscopic mode considers all of the failure processes occurring at the "local" level. Samples for observation in the SEM were obtained from the deformed and failed specimens by sectioning parallel to the fracture surface, i.e., slicing perpendicular to the major stress axis.

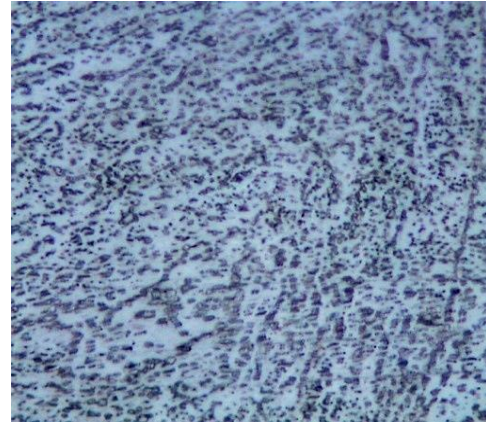
## **4. Results and discussion**

### **4.1 Initial microstructure**

The microstructure of this alloy steel sample is an important factor that essentially determines its hardness, tensile properties, cyclic fatigue resistance and eventual fracture behavior. The optical microstructure of this alloy steel in the longitudinal (L) orientation is shown in Fig. 1 and in the transverse (T) orientation in Fig. 2. The observed microstructure is typical of high strength alloy steels in that it reveals a combination of alloy-rich and alloy-depleted regions at the fine microscopic level. Being a vacuum melt product, the amount of such segregation on a gross scale is much less than one would expect in the air melt and cast product. However, at the fine microscopic level the segregation is still significant enough to have an impact on resistance to crack initiation. The local pockets of high alloy content in this steel resulted in the formation and presence of a noticeable volume fraction of martensite in these regions. The overall morphology of martensite in these alloy and carbon-rich regions was in the form of short and fine needle-like laths. These fine laths were intermingled with well-defined pockets of the ferrite-rich region, i.e., the base alloy material. The

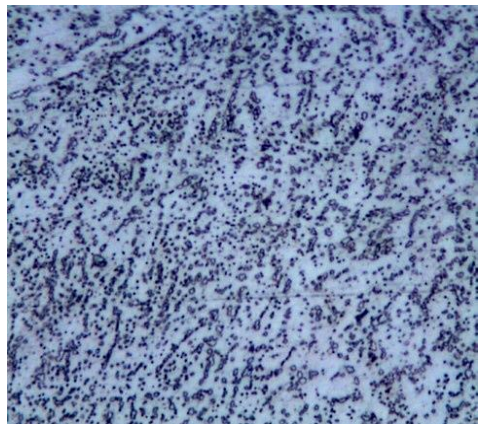


(a) Low magnification micrograph showing overall morphology

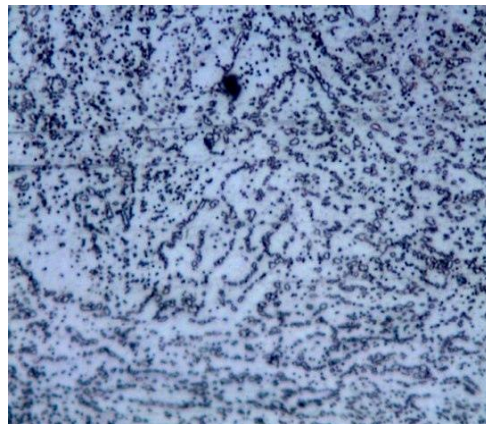


(b) High magnification observation of (a) showing morphology and distribution of the martensite

Fig. 1 Optical Micrographs showing the microstructure of X-2M sample in LONGITUDINAL orientation at two different magnifications



(a) Low magnification micrograph showing overall morphology



(b) High magnification observation of (a) showing morphology and distribution of the martensite

Fig. 2 Optical Micrographs showing the microstructure of X-2M sample in TRANSVERSE orientation at two different magnifications

presence of martensite micro-constituent in the alloy-rich regions is governed by a synergism of composition and processing technique used to engineer the starting material and does exert an influence on ‘local’ hardness, global tensile response and overall fracture behavior. In both the longitudinal (L) and transverse (T) samples, the volume fraction of the alloy and carbon-rich region was noticeably more than the alloy-depleted region. The presence and distribution of other second-phase particles in the microstructure of this steel but could not be easily identified at the allowable magnifications of the optical microscope. It is noted that the second-phase particles occur primarily in the matrix, i.e., alloy lean region, consistent with the fact that the alloy carbides deplete the surrounding matrix of alloy content.

Table 2 A compilation of the micro-hardness measurements made on X-2M [Load: 500gfDwell Time: 15 Seconds]

Orientation		Trial 1	Trial 2	Trial 3	Average Hardness kgf/mm <sup>2</sup>	Average Hardness GPa
Transverse	D1 $\mu\text{m}$	55.35	51.75	55.06	--	--
	D2 $\mu\text{m}$	57.7	55.06	46.51	--	--
	Hv, kgf/mm <sup>2</sup>	290	325	283	299	2.93
Longitudinal	D1 $\mu\text{m}$	44.62	44.76	49.13	--	--
	D2 $\mu\text{m}$	46.69	52.9	52.44	--	--
	Hv, kgf/mm <sup>2</sup>	445	389	359	398	3.90

#### 4.2 Hardness

The microhardness measurements were made, with both care and precision, from one edge to the other of the polished surface of both the longitudinal sample and the transverse sample of alloy steel X2M. Three measurements were made at different locations on the polished surface of each specimen to provide useful information pertaining to spatial variability of hardness. All of the measurements were made across the center of the sample that was mounted in bakelite in order to gather information on spatial variability of hardness while concurrently minimizing contributions from location of the indent. Making measurements on polished surface of the alloy steel sample facilitates in reducing spread in the measured hardness values. The micro-hardness provides a direct measure of the effect of strengthening arising from the presence of intrinsic micro constituents in the alloy steel microstructure and any concurrent softening or weakening arising due to the presence of defects in the microstructure, such as, fine microscopic voids and microscopic cracks. The microhardness values are summarized in Table 2. The hardness of the longitudinal specimen is 398 kgf/mm<sup>2</sup>, while average hardness of the transverse specimen is 299 kgf/mm<sup>2</sup>. A difference of 33 pct. in hardness was found between the two orientations.

#### 4.3 Tensile properties

The tensile properties of the X2M alloy steel, at ambient temperature (25°C), are summarized in Table 3. Results reported are the average values based on duplicate tests.

(a) The elastic modulus (E) of this alloy steel was 175 GPa in the longitudinal (L) direction and 150 GPa in the transverse (T) direction. The transverse (T) direction shows a decrease of 14 pct. in comparison with the longitudinal (L) direction. This may have important implications relative to optimal orientation and machining of the test specimen.

(b) The yield strength of this alloy steel in the longitudinal (L) direction [ $\sigma_{YS} = 371$  MPa] was forty percent higher than in transverse (T) yield strength [ $\sigma_{YS} = 264$  MPa].

(c) The ultimate tensile strength in the longitudinal (L) direction [ $\sigma_{UTS} = 638$  MPa] was twenty-two percent higher than the ultimate tensile strength in the transverse (T) direction [ $\sigma_{UTS} = 523$  MPa]. This substantiates the strong dependence on working direction coupled with distribution

Table 3 A compilation of room temperature ( $T = 25^{\circ}\text{C}$ ) tensile properties of alloy steel X-2M taken in both the longitudinal and transverse orientations (Results are mean values based on duplicate tests)

No.	Orientation	Elastic modulus		Yield Stress		Ultimate Stress		Ductility	Reduction in Area
		GPa	ksi	MPa	Ksi	MPa	Ksi		
1	Longitudinal	175	25.3	371	53.87	638	92.4	14.3	54.0
2	Transverse	150	21.8	264	38.22	523	75.8	17.2	60.0

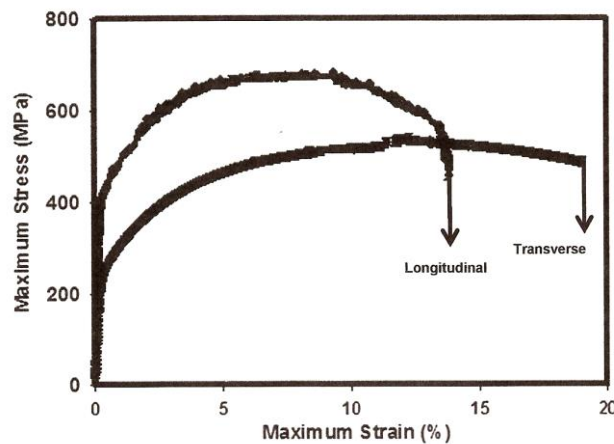


Fig. 3 A comparison of the engineering stress versus engineering strain curves for the longitudinal (L) and transverse (T) samples of X-2M deformed in uniaxial tension at room temperature ( $T = 25^{\circ}\text{C}$ ).

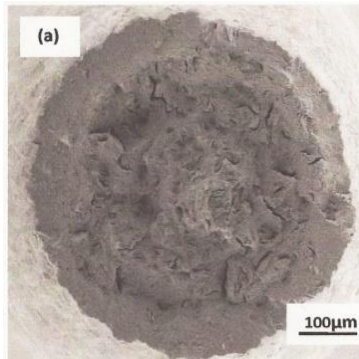
of second-phase particles in the microstructure and the resultant implications in processing of the final component of this steel

(d) In both the longitudinal (L) and transverse (T) directions the ultimate tensile strength ( $\sigma_{UTS}$ ) is higher than the tensile yield strength ( $\sigma_{YS}$ ) indicating the occurrence of significant strain hardening beyond yield.

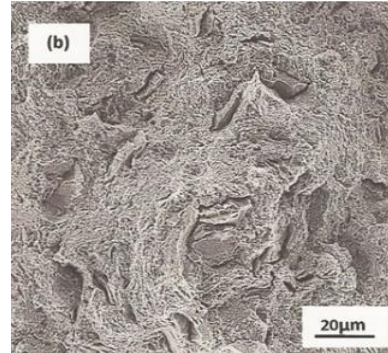
(e) The ductility quantified by elongation over 12.7 mm gage length was 14 percent in the longitudinal (L) direction and 17 percent in the transverse (T) direction. The observed higher ductility in the transverse direction is commensurate with the lower yield strength and tensile strength in this direction.

(f) The reduction in test specimen cross-section area, a direct measure of ductility, was 60 pct. in the transverse (T) direction and 54 pct. in the longitudinal (L) direction and reveals the same trend observed by the measurement of tensile elongation.

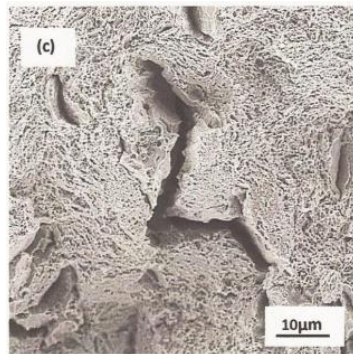
The engineering stress versus engineering strain curves for the two orientations are compared in Fig. 3. Both the longitudinal (L) and transverse (T) samples exhibit identical elastic behavior and near similar strain hardening characteristics. Immediately following the onset of necking, i.e., ultimate tensile strength, both the longitudinal (L) and transverse (T) samples of this alloy steel exhibited substantial plastic deformation and/or strain prior to failure.



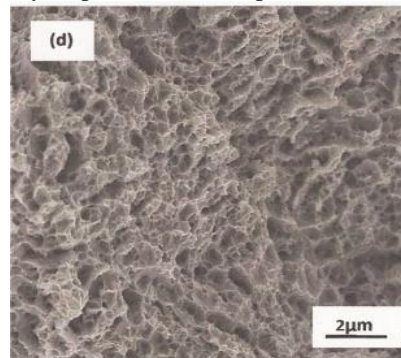
(a) Overall morphology of failure showing cup section of typical cup and cone fracture



(b) High magnification observation of (a) showing the transgranular region inlaid with randomly dispersed microscopic cracks



(c) High magnification observation of (b) showing microcrack leading in the formation of a macro-crack

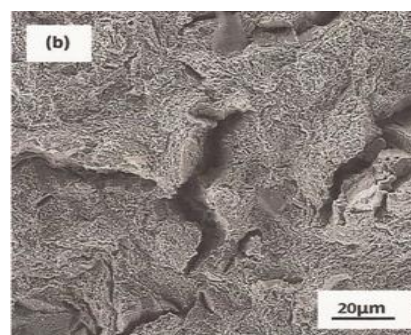


(d) Region showing the key microscopic features, namely microscopic voids and dimples, reminiscent of the occurrence of “locally” ductile failure mechanisms

Fig. 4 Scanning electron micrograph of the tensile fracture surface of Longitudinal Sample of X-2M alloy steel showing



(a) Overall morphology of failure



(b) The depth and severity of cracks both microscopic and macroscopic is in this micrograph

Fig. 5 Scanning electron micrograph of the tensile fracture surface of Transverse Sample of X-2M alloy steel showing

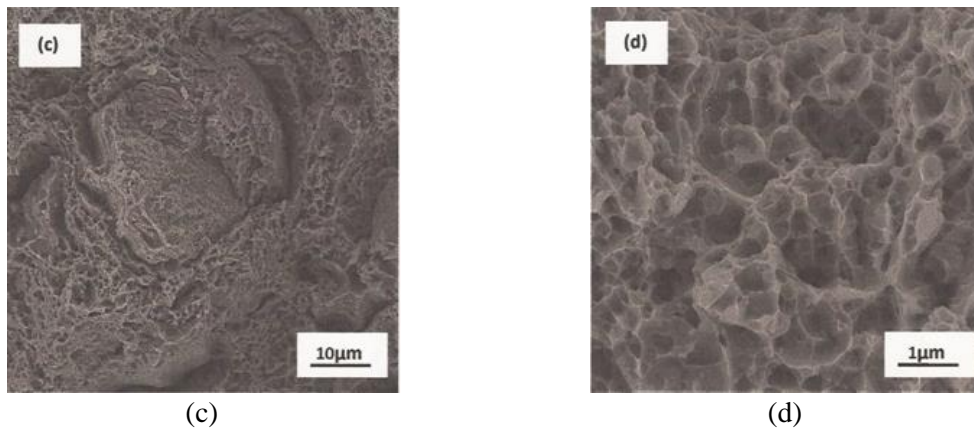


Fig. 5 Continued

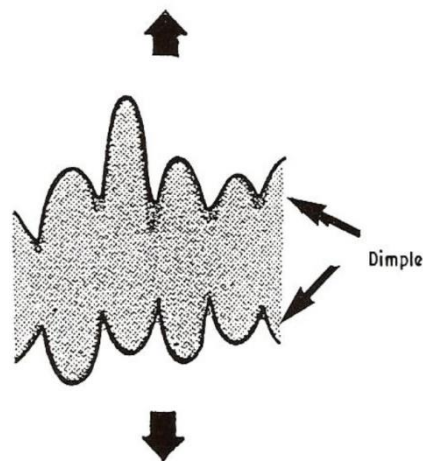


Fig. 7 Schematic representation of the dimples observed on the tensile fracture surface

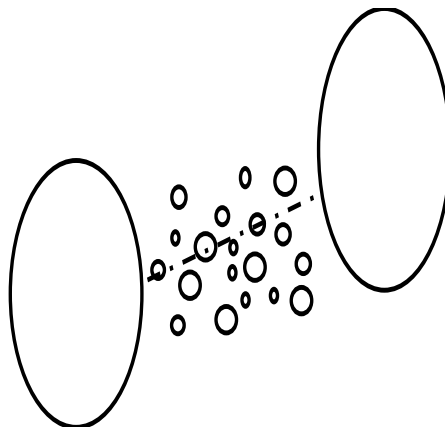


Fig. 7 Schematic showing the formation of void sheets between expanding or growing voids leading to void-void interactions and eventual coalescence

#### 4.4 Tensile fracture behavior

The tensile fracture surfaces of both the longitudinal (L) and transverse (T) specimens were examined in a scanning electron microscope to provide useful information relating to the specific role of intrinsic microstructural constituents and features on strength, ductility and fracture properties of the candidate steel. Representative micrographs for the two orientations are shown in Figs. 4 and 5.

##### 4.4.1 Longitudinal sample of steel X2M

Scanning electron microscopy observations of the tensile fracture surface revealed fracture to occur by characteristic “cup and cone” type of separation Fig. 4(a). Examination of the tensile fracture surface at gradually higher allowable magnifications of the SEM revealed the transgranular regions to be inlaid with a noticeable number of randomly dispersed microscopic cracks Fig. 4(b).

High magnification observation of the transgranular region revealed the nature and morphology of the fine microscopic cracks and their coalescence resulting in the formation and presence of a macroscopic crack Fig. 4(c). The region of tensile overload revealed a healthy and observable population of fine microscopic voids intermingled with well-defined dimples Fig. 4(d). These features are indicative of the locally operating ductile failure mechanisms and thus good overall toughness at the fine microscopic level. During far-field loading in tension the fine microscopic voids appeared to have undergone limited growth and with time they coalesce to form one or more fine microscopic cracks. Coalescence is aided by the linkage of the larger macroscopic voids with other finer and more closely spaced microscopic voids. The halves of these voids, both macroscopic and fine microscopic, are the dimples of varying size and shape visible in sizeable number on the tensile fracture surface Fig. 6.

##### 4.4.2 Tensile fracture of the transverse sample

Scanning electron microscopy observation of the tensile fracture surface of this sample revealed the occurrence of necking prior to failure and commensurate with the higher ductility of the steel sample in this direction Fig. 5(a). Higher allowable magnifications of the scanning electron microscope revealed a clear and distinct array of fine microscopic and macroscopic cracks Fig. 5(b). The region of tensile overload was covered with shallow dimples, cracks of varying size and shape, and fine microscopic voids Fig. 5(c). These features present on the overload surface provide reminiscence of the occurrence of both ductile and brittle failure mechanisms at the microscopic level. A sizeable fraction of the fracture surface was covered with well-defined array of voids intermingled with dimples Fig. 5(d). Coalescence of the macroscopic voids is facilitated by the formation of void sheets that is aided by the intense localization of strain that is present between neighboring voids Fig. 7. Half of the fine microscopic void is the dimple clearly visible in large numbers on the tensile fracture surface.

#### 4.5 Microscopic mechanisms governing stress-microstructure interactions and fracture

During gradual loading in uniaxial tension the initiation and gradual build-up of dislocations at the grain boundaries and other second-phase particles to include the fine laths of martensite present and distributed through the microstructure does assist in the early initiation of fine microscopic voids at the second-phase particles in the microstructure. This occurs when the “local” strain caused by the gradual pile-up of dislocations at an interface of the second-phase particle with the matrix

reaches a “locally” high value. Void initiation at the coarse second-phase particle is favored to occur following the onset of yielding and at low values of plastic strain. During continued loading in tension a few of the second-phase particles present in the microstructure are assumed to fail by fracture on account of their intrinsic brittleness. Since an extension of the crack during tensile loading is favored to occur at the prevailing high “local” stress intensities comparable to the fracture toughness of the material, the presence of both macroscopic and fine microscopic voids contributes to degrading the actual strain-to-failure associated with ductile fracture (Tvergaard 2002, Tvergaard 2008).

In essence, the observed presence of a noticeable number of fine microscopic voids essentially transforms the deforming alloy steel into a “composite” material at the fine microscopic level. The composite comprising of two populations of particles, namely: (a) the grains in the matrix and (b) voids [the void now being considered to be a particle having zero stiffness]. Since the voids are intrinsically softer than the steel matrix, the ‘local’ strain tends to get significantly elevated both at and around the region of a microscopic void. This results in conditions conducive for an increase in their volume fraction. During continued loading in the tensile direction the fine microscopic voids grow. The voids grow until coalescence is favored to occur by mutual interaction and/or impingement through the formation of void-sheets Fig. 7. Failure of the void sheet occurs in a manner that results in a rough fracture surface at the fine microscopic level. Half of the void is the shallow dimples, observed in sizeable number, on the tensile fracture surface of both the longitudinal (L) and transverse (T) samples.

## 5. Conclusions

Based on a comprehensive study on understanding the specific influence of composition and processing on microstructure, hardness and tensile response of alloy steel X2M, following are key findings:

- Optical microstructure of this alloy steel revealed a combination of alloy-rich and alloy-depleted region. Local regions having high alloy content in this steel resulted in a greater volume fraction of martensite in these regions. The presence and overall morphology of martensite was in the form of short and fine needles or ‘lath’. The fine laths were intermingled with pockets of ferrite-rich matrix. The grains were elongated along the longitudinal direction of the as-provided material and so also were the observed distribution of the second phase alloy carbide particles.

- The microhardness measurements were consistent in a given orientation. This alloy steel revealed marginally greater micro-hardness along the longitudinal (L) orientation [398 kgf/mm<sup>2</sup>] than in the transverse (L) orientation [299 kgf/mm<sup>2</sup>]. The difference in hardness between the two orientations was as high as 99 kgf/m<sup>2</sup> i.e., 0.97 GPa or 33 pct.

- The elastic modulus of this alloy steel was noticeably different in the two orientations longitudinal and transverse. The modulus in the transverse direction (150 GPa) was fourteen percent lower than the elastic modulus in longitudinal direction (175 GPa).

- The yield strength in the longitudinal; (L) orientation was forty percent more than in the transverse orientation [264 MPa]. The ultimate tensile strength in the longitudinal orientation [638 MPa] is twenty percent higher than in the transverse orientation [523 MPa].

- The ductility quantified by elongation over 0.5 inch (12.7 mm) gage length was highest in the transverse (T) orientation than in the longitudinal (L) orientation. The observed higher ductility is

consistent with the lower yield strength and tensile strength in the transverse orientation.

- The reduction in test specimen cross-section area was higher in the transverse (T) orientation (60 pct.) than in the longitudinal orientation (54 pct.) and follows the same trend shown by tensile elongation.

- Tensile fracture was macroscopically ductile following a cup and cone failure. Microscopically the fracture surface revealed an observable number of fine microscopic cracks, few macroscopic cracks, population of voids and dimples; features reminiscent of locally brittle and ductile failure mechanisms.

## Acknowledgment

This research was made possible through material provided by Deformation Control Technology Inc (Cleveland, OH, USA). Mr. ManigandanKannan (*Graduate student*: Department of Mechanical Engineering, The University of Akron) extends thanks and appreciation to the University for providing support through tuition scholarship.

## References

- Askeland, D.R. and Phulke, P.P. (2008), *The Science and Engineering of Materials*, Fifth Edition, Thompson Publishers, USA, 2005, 520-530.
- Averbach, B.L., Bingzhe Lou, Pearson, P.K., Fairchild, R.E. and Bamberger, E.N. (1985), "Fatigue crack propagation in carburized high alloy bearing steels", *Metall. Transact.*, **16A**, 1253-1259.
- Averbach, B.L., Bingzhe Lou, Pearson, P.K., Fairchild, R.E. and Bamberger, E.N. (1985), "Fatigue crack propagation in carburized X-2M steel", *Metall. Transact.*, **16A**, 1267-1272.
- Bajer, A.J., Laura, E.J. and Wei, R.P. (1965), *Structure and Properties of Ultrahigh Strength Steels*, ASTM STP 370, ASTM, Philadelphia, PA, 3-13.
- Bucher, J.H., Powell, G.W. and Sputnik, J.W. (1966), *Application of Fracture Toughness Parameters to Structural Metals*, edited by Herman Greenberg, Gordon and Breach, New York, USA.
- Cunningham, R.J. (1974), *Boeing-Vertol Division of Boeing Company, "Steel (X2M) Transmission Gear Material Evaluation*, Test Results and Final Report, U.S. Government Contract No. DAAJ01 70-C-0840.
- Cunningham, R.J. (1975), "Process for Carburizing High Alloy Steels", U.S. Patent Number 3,885,995.
- Danzeisen, J., Merklein, M. and Roll, K. (2008), "Investigation of fracture behavior of TRIP steels", *Int. J. Mater. Form. Suppl.*, **1**, 221-224
- Dieter, G.E. (2006), *Mechanical Metallurgy*, Third Edition, McGraw Hill Publishers, 400-410.
- Kanvinde, A.M. and Deierlein, G.G. (2007), "Cyclic void growth model to assess ductile fracture initiation in structural steels during low cycle fatigue", *J. Eng. Mech.*, 701-712.
- Pascover, J.S. and Malas, S.J. (1965), *Structure and Properties of Ultra-High Strength Steels*, ASTM STP 370, ASTM, Philadelphia, USA, 370-389.
- Thomas, G., Schmatz, D. and Gerberich, W.W. (1965), in *High Strength Materials* (Edited by V.F. Zackay), John Wiley and Sons, New York, USA, 199-219.
- Townsend, D.P., and Zaretsky, E.V. (1980), Report NASA-TP-1731 (N81-14322), Lewis Research Center, Cleveland, Ohio.
- Tvergaard, V. (2008), "Shear deformation of voids modeled by internal pressure", *Int. J. Mech. Sci.*, **50**, 1459-1465.
- Tvergaard, V. and Hutchinson, J.W. (2002), "Material failure by void growth to coalescence", *Int. J. Solids Struct.*, **39**(13-14), 3581-3597.

- Van Slycken, J., Verleysen, P. and Degrieck, J. (2006), "High Strain rate behavior of low alloy multiphase aluminum- and silicon-based transformation-induced plasticity steels", *Metall. Mater. Transact.*, **37A**, 1537-1539.
- Van Slycken, J., Verleysen, P. and Degrieck, J. (2007), "Dynamic response of aluminum-containing TRIP steel and its constituent phases", *Mater. Sic. Eng.*, A460-461, 516-524.